Supporting Information

High-Performance Ultra-Flexible Organic Solar Cells Enabled by Transfer-Free Polyimide/ITO Integrated Electrodes

Jingyang Xiao,[‡*ab] Jilong Yu,[‡a] Mingzhou Luo,[a] Wenlong Wu,[a] Kang An,[c] Chen Zhao,[ab] Wan-Yi Tan[ab] and Yonggang Min[*ab]

[a] School of Materials and Energy, Guangdong University of Technology, Guangzhou 510006, China

[b] Guangdong Provincial Laboratory of Chemistry and Fine Chemical Engineering Jieyang Center, Jieyang, 515200, China

[c] State Key Laboratory of Luminescent Materials and Devices, School of Materials Science and Engineering, South China University of Technology, Guangzhou 510640, China

[‡] J. Xiao and J. Yu contributed equally to this work.
[*] Corresponding author.
E-mail: xiaojingyang@gdut.edu.cn (J. Xiao), ygmin@gdut.edu.cn (Y. Min).

1. Experimental Section

Materials

The borosilicate glass was purchased from Luoyang Tengjing Co., Ltd. PET/ITO and glass/ITO substrates (15 Ω/□) were purchased from Advanced Election Technology Co., Ltd. PM6 was purchased from Hyper PV Technology. Co., Ltd, while Y6 and PDIN were purchased from Solarmer Materials Inc. 2,2′-Bis(trifluoromethyl)benzidine (TFMB), 3,3',4,4'-Biphenyl tetracarboxylic dianhydride (BPDA) were purchased from J&K Scientific and Huimai Material Technology Co., Ltd., respectively. All chemicals were used as received without further purification.

Synthesis of Colorless Polyimide (PI)

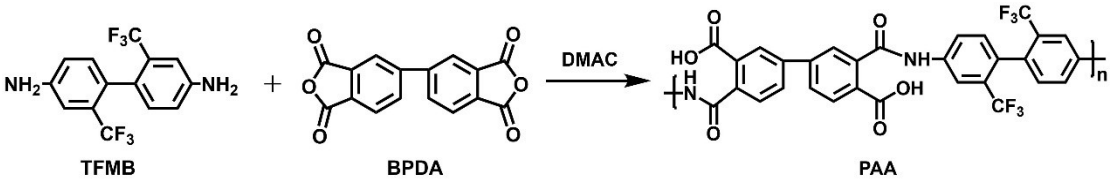

Scheme 1. Synthetic route for the PI precursor.

A typical two-step method was employed to synthesize colorless PI films, with a simple process similar to previous reports.[1] Taking poly(amidic acid) (PAA) precursor solution with 25% solid content as an example, 3.2 g of TFMB and 2.9422 g of BPDA (molar ratio = 1:1) were introduced into a three-neck, round-bottomed flask filled with 18.4266 g of N,N-dimethylacetamide (DMAc) solvent, followed by stirring at room temperature for 8 hours. The resulting mixture was then subjected to vacuum defoaming to obtain a colorless PAA solution. The as-prepared PAA solution was spin-coated onto clean borosilicate glass substrates and pre-cured at 120°C for 30 min. Subsequently, a stepwise thermal annealing process was conducted in a muffle furnace

under nitrogen atmosphere to obtain PI films: the temperature was raised from room temperature to 300°C with a heating rate of 5°C/min, and then maintained for 80 min to complete imidization.

Device fabrication

For the PI/ITO integrated transparent electrode, an ITO layer was deposited onto the PI film via magnetron sputtering method, following by thermal annealing at 250 °C for 30 min. The as-prepared PI/ITO substrate, commercially purchased PET/ITO and glass/ITO substrates were cleaned sequentially with detergent, deionized water and ethanol under sonication for 30 min each and dried at 60 °C in an oven overnight, followed by an oxygen plasma treatment of 10 min. A hole transport layer (HTL) was prepared by spin-coating PEDOT:PSS 4083 at 3000 rpm for 30 s onto the cleaned PI/ITO substrate. This was followed by thermal annealing in air, at 150 °C for 15 min. Afterwards, the substrates were transferred into an N_2-filled glovebox. The PM6:Y6 blend solution (CF, 1:1.2 by weight, 6.5 mg/mL for PM6) was spin-coated at 3000 rpm for 30 s to form the photoactive layer, which was then thermal annealed on a hotplate at 110 °C for 10 min. Subsequently, a thin layer of electron transporting layer was deposited by spin-coating a methanol solution of PDIN (2 mg/mL) at 3000 rpm for 30 s onto the active layers. Finally, 100 nm of Ag electrode was thermally evaporated onto the device under vacuum. Prior to the Ag deposition, a shadow mask was carefully aligned onto the samples to define an active area of 0.0516 cm^2.

Measurements and Instruments

***J-V* and EQE measurement**

The current density-voltage (*J-V)* characteristics were measured by a Keithley

2400 source meter, under 1 sun irradiation (AM 1.5G, 100 mW cm^{-2}) using a solar simulator (XES-50S1, SAN-EI ELECTRIC, Japan). Before the *J-V* tests, a physical mask with an aperture with precise area of 0.04 cm^2 was used to define the device area. The external quantum efficiency (EQE) curves were measured by an integrated QE measurement system (Enlitech, Taiwan, China).

Optical transmission spectra

The optical transmission spectra of transparent electrodes on a quartz substrate were recorded by SHIMADZU UV-3600 Plus.

AFM characterization

The AFM height and phase images were obtained by a Bruker Dimension Fast Scan.

SEM characterization

The SEM images were obtained by an Apreo 2S HiVac scanning electron microscope (Thermo Fisher Scientific Brno s.r.o., Czech Republic).

2. Supplementary Figures

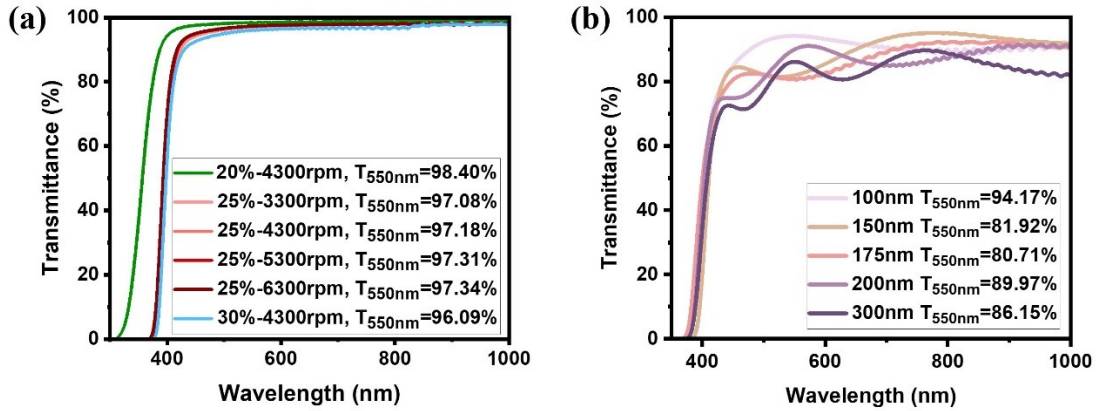

Figure S1. a) Transmittance of PI substrates fabricated with various spin-coating speeds and solid contents; b) Transmittance of PI/ITO integrated electrodes with various ITO thicknesses.

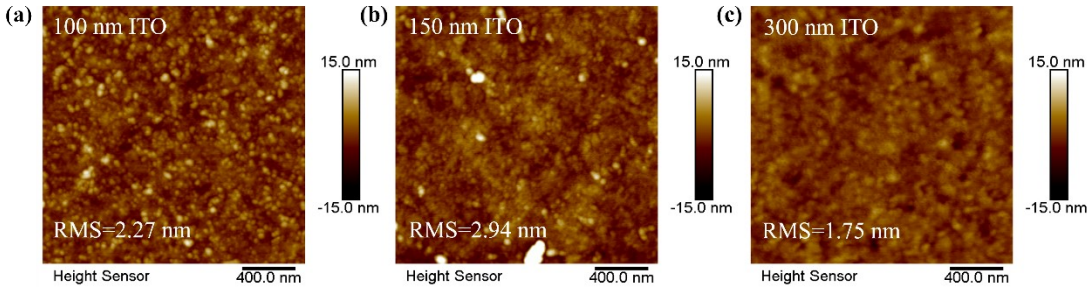

Figure S2. a) AFM images of PI/ITO integrated electrodes with ITO thickness of a) 100 nm; b) 150 nm; c) 300 nm.

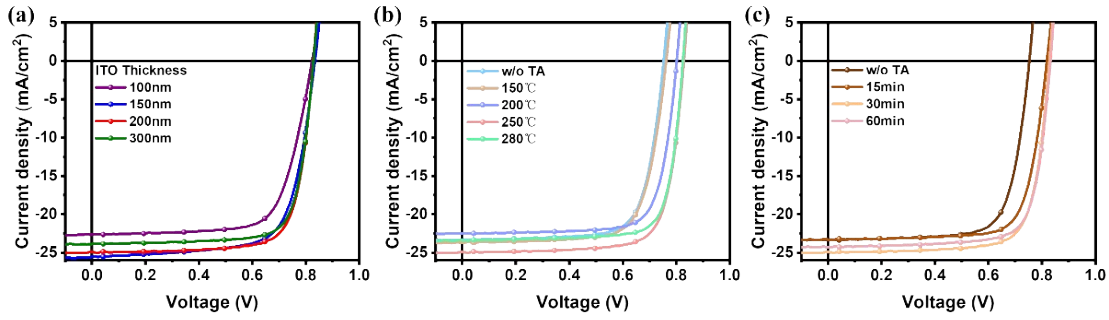

Figure S3. J-V characteristics of PI/ITO-based OSCs a) with different ITO thicknesses; b) with different thermal annealing temperatures for ITO; c) different thermal annealing durations for ITO.

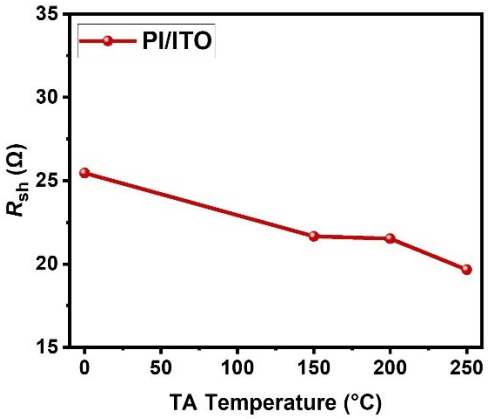

Figure S4. Variation of sheet resistance of PI/ITO electrodes with thermal annealing at different temperatures.

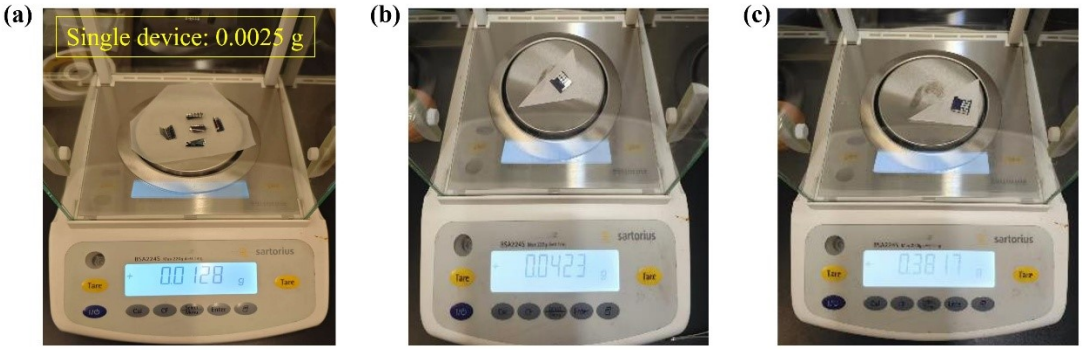

Figure S5. The images of OSC devices based on a) PI, b) PET, and c) glass substrates. Note: the average weight of a single PI-based device is 0.0025 g.

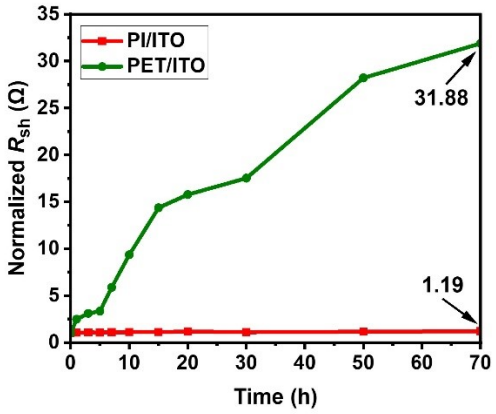

Figure S6. Normalized sheet resistance of different flexible transparent electrodes versus thermal annealing time.

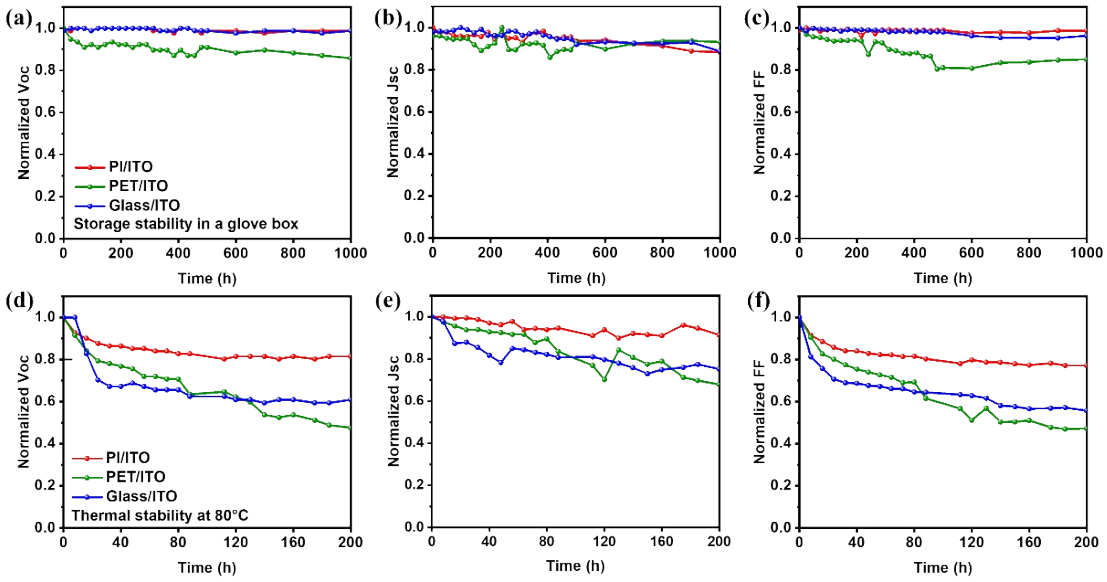

Figure S7. Normalized photovoltaic parameters of the OSCs fabricated with different transparent electrodes a-c) during storage stability test in an N_2-filled glovebox; d-f) under thermal stress at 80 °C.

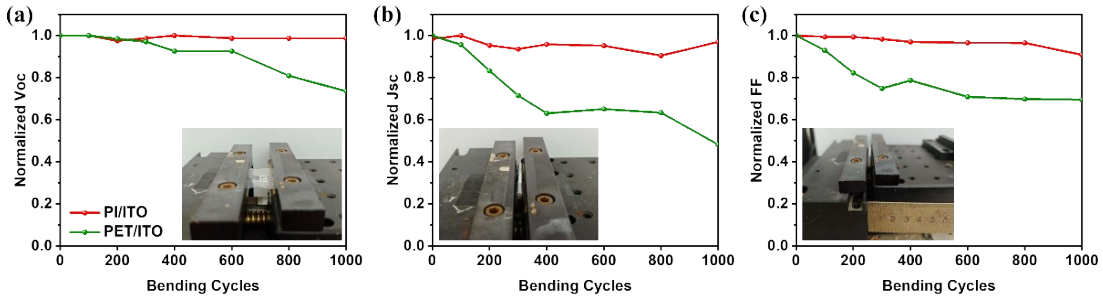

Figure S8. Normalized photovoltaic parameters of the OSCs fabricated with different transparent electrodes after various bending cycles with a bending radius of 4 mm. (Inserted images display the flat and bended states of flexible devices during the bending test.)

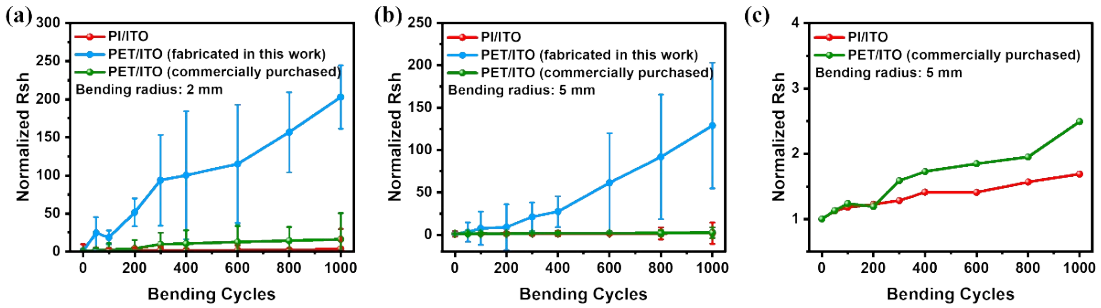

Figure S9. Normalized sheet resistance of different flexible transparent electrodes after various bending cycles at a bending radius of a) 2 mm; b, c) 5 mm.

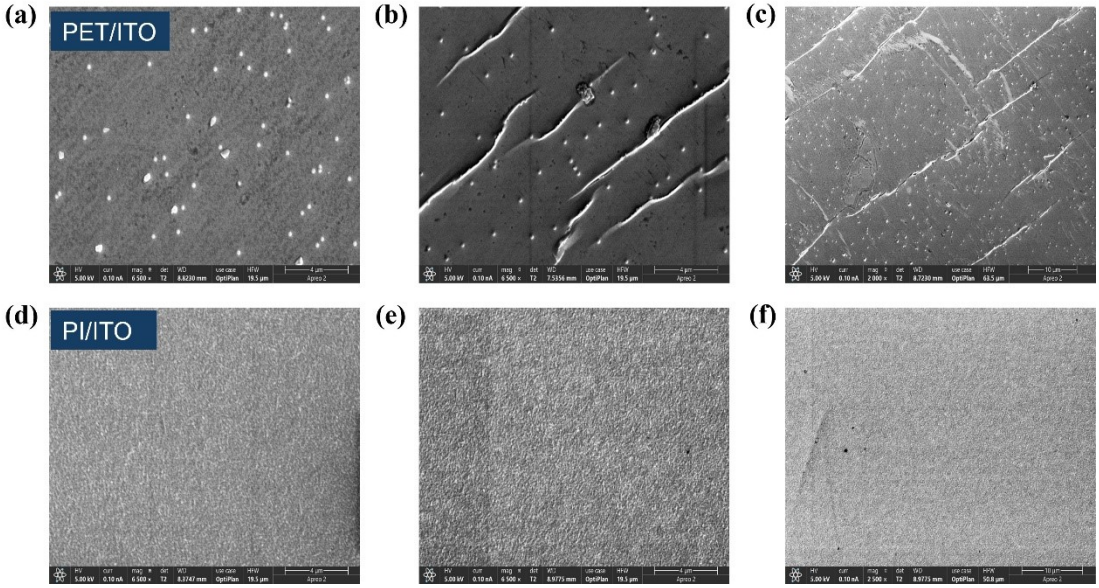

Figure S10. SEM image of PET/ITO (a) before and (b, c) after 500 bending cycles at a bending radius of 2 mm; SEM image of PI/ITO (d) before and (e, f) after the same bending test. The images are recorded at a scale of (a, b, d, e) 4 μm and (c, f) 10 μm.

3. Supplementary Tables

Table S1. Film thickness of PI substrates fabricated with various spin-coating speeds and solid contents.

Solid Content (%)	Spin-coating Speed (rpm)	Film Thickness (μm)
20	6300	/
25	3300	11
	4300	9
	5300	7
	6300	5
30	3300	17
	4300	15
	5300	13
	6300	11

Table S2. Sheet resistances of PI/ITO integrated electrodes with various ITO thicknesses, measured by four-point probe technique.

Thickness (nm)	100	150	175	200	300
R_1 (Ω)	47.5	33.5	29.95	20.6	22.1
R_2 (Ω)	44.3	28	26.55	21.3	17.2
R_3 (Ω)	48.5	30.1	28.57	21.8	21.4
R_4 (Ω)	51.4	29.4	27.83	22	20.9
R_5 (Ω)	52.1	30.9	28.26	19.7	18.7
R_6 (Ω)	56.7	33.7	28.30	22.6	18.8
R_7 (Ω)	45.2	28.4	26.48	19.1	16.5
R_8 (Ω)	50.8	32.6	28.94	22.2	23.4
R_9 (Ω)	57.1	34.1	33.55	24.5	20.1
R_{10} (Ω)	53.0	30.5	31.30	22.4	19.5
Average R_{sh} (Ω)	50.66	31.12	28.97	21.62	19.86

Table S3. Photovoltaic parameters of PI/ITO-based OSCs with different ITO thicknesses, measured under AM 1.5G irradiation.

Thickness (nm)	V_{OC}[a)] (V)	J_{SC}[a)] (mA·cm^{-2})	FF[a)] (%)	PCE[a)] (%)
100	0.82 (0.82±0.00)	25.02 (24.76±0.32)	67.20 (67.05±3.24)	13.74 (13.62±0.79)
150	0.83 (0.83±0.00)	25.55 (24.81±0.61)	71.12 (71.78±1.97)	15.16 (14.82±0.28)
200	0.83 (0.83±0.01)	24.93 (24.74±0.36)	76.23 (75.60±1.00)	15.75 (15.45±0.18)
300	0.83 (0.83±0.00)	23.88 (23.57±0.25)	76.89 (75.88±1.07)	15.22 (14.79±0.20)

a) The values in parentheses represent statistical data obtained from ten devices.

Table S4. Photovoltaic parameters of PI/ITO-based OSCs with different thermal annealing temperatures for ITO, measured under AM 1.5G irradiation.

TA temperature (°C)	V_{OC}[a)] (V)	J_{SC}[a)] (mA·cm^{-2})	FF[a)] (%)	PCE[a)] (%)
w/o annealing	0.75 (0.75±0.01)	23.56 (23.00±0.56)	73.81 (71.62±2.66)	13.00 (12.31±0.87)
150°C	0.77 (0.77±0.01)	23.67 (22.47±0.61)	73.36 (73.94±0.75)	13.24 (12.72±0.29)
200°C	0.80 (0.79±0.02)	22.51 (23.09±0.79)	76.16 (75.04±1.21)	13.76 (13.62±0.11)
250°C	0.83 (0.83±0.01)	24.93 (24.74±0.36)	76.23 (75.60±1.00)	15.75 (15.45±0.18)
280°C	0.82 (0.82±0.00)	23.39 (23.19±0.35)	78.02 (76.70±0.78)	15.05 (14.60±0.31)

a) The values in parentheses represent statistical data obtained from ten devices.

Table S5. Photovoltaic parameters of PI/ITO-based OSCs with different thermal annealing durations for ITO, measured under AM 1.5G irradiation.

TA time	V_{OC}[a)] (V)	J_{SC}[a)] (mA·cm^{-2})	FF[a)] (%)	PCE[a)] (%)
w/o annealing	0.75 (0.75±0.01)	23.56 (23.00±0.56)	73.81 (71.62±2.66)	13.00 (12.31±0.87)
15 min	0.82 (0.83±0.01)	23.29 (22.48±1.13)	75.63 (72.86±2.20)	14.43 (13.56±0.64)
30 min	0.83 (0.83±0.01)	24.93 (24.74±0.36)	76.23 (75.60±1.00)	15.75 (15.45±0.18)
60 min	0.83 (0.83±0.01)	24.29 (23.89±0.62)	76.40 (75.08±1.44)	15.44 (14.89±0.38)

a) The values in parentheses represent statistical data obtained from ten devices.

Table S6. Photovoltaic parameters of the reported flexible OSCs based on PM6:Y6.

Device	Electrode	Thickness (μm)	V_{OC} (V)	J_{SC} (mA·cm^{-2})	FF (%)	PCE (%)	Ref
Rigid	Glass/ITO	/	0.84	24.89	74.37	15.75	[2]
Flexible	PET/PH1000	/	0.83	23.57	72.03	14.07	
Rigid	Glass/ITO	/	0.84	25.53	67.80	14.47	[3]
Flexible	Flexible/AgNWs-GV	125	0.84	23.54	73.20	14.42	
Rigid	Glass/ITO	/	0.83	25.43	74.50	15.71	[4]
Flexible	PET/FlexAgNE/ZnO	125	0.83	24.87	74.30	15.32	
Rigid	Glass/ITO	/	0.82	25.9	73	15.4	[5]
Flexible	PI/ITO	1.4	0.83	25.7	72	15.2	
Flexible	PET/AgNWs/ZnO:PVP	125	0.82	24.58	74.45	15.01	[6]
Rigid	Glass/ITO	/	0.84	25.67	72	15.43	[7]
Flexible	PEN/PEDOT:PSS	1.3	0.84	25.36	70	15.03	
Flexible	PEN/AgNWs	125	0.83	25.40	71	15.03	[8]
Rigid	Glass/ITO	/	0.83	25.66	73.75	15.78	[9]
Flexible	Em-Ag/AgNWs:AZO-SG	125	0.83	25.05	72.97	15.21	
Flexible	PET/PEDOT:PSS	125	0.83	24.80	66.00	13.62	[10]
Rigid	Glass/ITO	/	0.84	26.78	71.43	16.08	[11]
Flexible	PET/PEDOT:PSS	/	0.83	23.21	68.63	12.59	
Rigid	Glass/ITO	/	0.85	25.00	74.00	15.70	[12]
Flexible	PI/Graphene	25	0.84	25.80	70.20	15.20	
Flexible	PI/AgNW	20	0.82	24.71	66.17	13.40	[13]
Rigid	Glass/ITO	/	0.83	25.81	74.94	16.05	This work
Flexible	PI/ITO/PEDOT:PSS	5	0.83	25.44[a]	76.23	16.10	

[a] The integrated J_{SC} derived from EQE measurement.

References

[1] Y. Wang, Q. Chen, G. Zhang, C. Xiao, Y. Wei, W. Li, Ultrathin Flexible Transparent Composite Electrode via Semi-embedding Silver Nanowires in a Colorless Polyimide for High-Performance Ultraflexible Organic Solar Cells, ACS Appl. Mater. Interfaces 14 (4) (2022) 5699-5708.

[2] T. Yan, W. Song, J. Huang, R. Peng, L. Huang, Z. Ge, 16.67% Rigid and 14.06% Flexible Organic Solar Cells Enabled by Ternary Heterojunction Strategy, Adv. Mater. 31 (39) (2019) 1902210.

[3] Z. Wang, Y. Han, L. Yan, C. Gong, J. Kang, H. Zhang, X. Sun, L. Zhang, J. Lin, Q. Luo, C. Q. Ma, High Power Conversion Efficiency of 13.61% for 1 cm2 Flexible Polymer Solar Cells Based on Patternable and Mass‐Producible Gravure‐Printed Silver Nanowire Electrodes, Adv. Funct. Mater 31 (4) (2021) 2007276.

[4] Y. Sun, L. Meng, X. Wan, Z. Guo, X. Ke, Z. Sun, K. Zhao, H. Zhang, C. Li, Y. Chen, Flexible High‐Performance and Solution‐Processed Organic Photovoltaics with Robust Mechanical Stability, Adv. Funct. Mater 31 (16) (2021) 2010000.

[5] S. Xiong, K. Fukuda, S. Lee, K. Nakano, X. Dong, T. Yokota, K. Tajima, Y. Zhou, T. Someya, Ultrathin and Efficient Organic Photovoltaics with Enhanced Air Stability by Suppression of Zinc Element Diffusion, Adv. Sci. 9 (8) (2022) 2105288.

[6] Z. Wang, J. Guo, Y. Pan, J. Fang, C. Gong, L. Mo, Q. Luo, J. Lin, C. Ma, Manipulating the Macroscopic and Microscopic Morphology of Large‐Area Gravure‐Printed ZnO Films for High‐Performance Flexible Organic Solar Cells, Energy Environ. Mater. 7 (2) (2023) e12592.

[7] Y. Li, R. Wen, P. Li, X. Fan, Metallic and Low-Work-Function PEDOT:PSS Cathodes for Flexible Organic Solar Cells Exhibiting Over 15% Efficiency and High Stability, ACS Appl. Energy Mater. 5 (6) (2022) 7692-7700.

[8] F. Qin, W. Wang, L. Sun, X. Jiang, L. Hu, S. Xiong, T. Liu, X. Dong, J. Li, Y. Jiang, J. Hou, K. Fukuda, T. Someya, Y. Zhou, Robust metal ion-chelated polymer interfacial layer for ultraflexible non-fullerene organic solar cells, Nat. Commun. 11 (1) (2020) 4508.

[9] X. Chen, G. Xu, G. Zeng, H. Gu, H. Chen, H. Xu, H. Yao, Y. Li, J. Hou, Y. Li, Realizing Ultrahigh Mechanical Flexibility and >15% Efficiency of Flexible Organic Solar Cells via a “Welding” Flexible Transparent Electrode, Adv. Mater. 32 (14) (2020) 1908478.

[10] R. Wen, H. Huang, J. Wan, S. Wen, J. Wang, X. Fan, High-Efficiency Stable Flexible Organic Solar Cells with PEDOT:PSS Electrodes via Superacid Fumigation Treatment, Energy Technol. 9 (11) (2021) 2100595.

[11] V. G. Sree, T. Gokulnath, B. Yadagiri, J. I. Sohn, H.-S. Kim, C. Bathula, Highly efficient halogen-free rigid and flexible binary organic solar cells using new solid indacene additive, Mater. Today Phys. 47 (2024) 101538.

[12] D. Koo, S. Jung, J. Seo, G. Jeong, Y. Choi, J. Lee, S. M. Lee, Y. Cho, M. Jeong, J. Lee, J. Oh, C. Yang, H. Park, Flexible Organic Solar Cells Over 15% Efficiency with Polyimide-Integrated Graphene Electrodes, Joule 4 (5) (2020) 1021-1034.

[13] Z. Shen, X. Liang, Y. Fan, G. Lin, T. Gu, H. Huo, Y. Wang, Z. Tang, W. Su, X. Xu, L. Hou, Ultra-flexible high-efficiency organic solar cells based on polyimide electrodes and all-polymer blends, Appl. Phys. Lett. 126 (10) (2025) 103301.